CORE
Metadata, citation and similar papers at core.ac.uk
Provided by Research Online

University of Wollongong
Research Online

Australian Institute for Innovative Materials - Papers
Australian Institute for Innovative Materials

1-1-2019

Zn-Doped Cu(100) facet with efficient catalytic ability for the CO2 electroreduction to ethylene

Yuefeng Zhang
Hunan University

Yong Zhao
University of Wollongong, yz705@uowmail.edu.au

Caiyun Wang
University of Wollongong, caiyun@uow.edu.au

Zengxi Wei
Hunan University

Junliang Yang
Central South University

See next page for additional authors

Follow this and additional works at: https://ro.uow.edu.au/aiimpapers

 Part of the Engineering Commons, and the Physical Sciences and Mathematics Commons

Recommended Citation

Zhang, Yuefeng; Zhao, Yong; Wang, Caiyun; Wei, Zengxi; Yang, Junliang; and Ma, Jianmin, "Zn-Doped Cu(100) facet with efficient catalytic ability for the CO2 electroreduction to ethylene" (2019). *Australian Institute for Innovative Materials - Papers*. 3839.
https://ro.uow.edu.au/aiimpapers/3839

Research Online is the open access institutional repository for the University of Wollongong. For further information contact the UOW Library: research-pubs@uow.edu.au

Zn-Doped Cu(100) facet with efficient catalytic ability for the CO2 electroreduction to ethylene

Abstract

Electrochemically converting CO2 into fuels and chemicals is an appealing strategy to create energy rich products. The highly demanded product ethylene has been preferably produced on Cu-based catalysts with abundant exposed Cu(100) facets. However, the performance is still limited by the large energy barrier for the C-C dimerization. Here, to lower the energy barrier, we tailor the electronic structure of Cu(100) by doping a series of transition metals using the density functional theory (DFT) method. The zinc-doped Cu(100) surface has shown a superior catalytic performance. Mechanistic study further reveals that doping with Zn alters the electronic structure around Cu, adjusts the atomic arrangement in the active sites and makes the catalyst surface electronegative, which is conducive to the activation of acidic molecular CO2 and the reduction of the energy barrier for C-C dimerization. This work reveals that the doping of Cu with transition metals has great potential in promoting the electrochemical CO2-to-C2H4 conversion. This work also provides deep insights into the formation mechanisms of C2H4, thus guiding the design of Cu-based bimetallic catalysts for its effective production.

Keywords

co2, electroreduction, zn-doped, ethylene, cu(100), facet, efficient, catalytic, ability

Disciplines

Engineering | Physical Sciences and Mathematics

Publication Details

Zhang, Y., Zhao, Y., Wang, C., Wei, Z., Yang, J. & Ma, J. (2019). Zn-Doped Cu(100) facet with efficient catalytic ability for the CO2 electroreduction to ethylene. Physical chemistry chemical physics : PCCP, 21 (38), 21341-21348.

Authors

Yuefeng Zhang, Yong Zhao, Caiyun Wang, Zengxi Wei, Junliang Yang, and Jianmin Ma

This journal article is available at Research Online: https://ro.uow.edu.au/aiimpapers/3839

Zn-Doped Cu(100) Facet with Efficient Catalytic Ability for the CO_2 Electroreduction to Ethylene

Yuefeng Zhang[§,a] Yong Zhao[§,b] Caiyun Wang,[b,*] Zengxi Wei,[a] Junliang Yang[c] and Jianmin Ma[a,d,e,*]

[a]School of Physics and Electronics, Hunan University, Changsha, 410082, PR China

[b]ARC Centre of Excellence for Electromaterials Science, Intelligent Polymer Research Institute, University of Wollongong, New South Wales, 2522, Australia

[c]Hunan Key Laboratory for Super-microstructure and Ultrafast Process, School of Physics and Electronics, Central South University, Changsha 410083, China

[d]Key Laboratory of Materials Processing and Mold (Zhengzhou University), Ministry of Education, Zhengzhou University, Zhengzhou 450002, China

[e]State Key Lab of Chemical Engineering, School of Chemical Engineering and Technology, Tianjin University, 300072, China

*Corresponding authors: caiyun@uow.edu.au; nanoelechem@hnu.edu.cn

§: Equal contribution.

Abstract

Electrochemically converting CO_2 into fuels and chemicals is an appealing strategy to create energy rich products. The highly demanded product ethylene has been preferably produced on Cu-based catalysts with abundant exposed Cu(100) facets. However, the performance is still limited by the large energy barrier for the C-C dimerization. Here, to lower the energy barrier, we tailor the electronic structure of Cu(100) by doping a series of transition metals using density functional theory (DFT) method. The zinc-doped Cu(100) surface has shown a superior catalytic performance. Mechanistic study further reveals that the doping with Zn alters the electronic structure around Cu, adjusts the atomic arrangement in the active sites and makes the catalyst surface electronegative, which is conducive to the activation of acidic molecular CO_2 and the reduction of energy barrier for C-C dimerization. This work reveals that the doping of Cu with transition metals has great potential in promoting the electrochemical CO_2-to-C_2H_4 conversion. This work also provides deep insights into the formation mechanisms of C_2H_4, and thus guiding the design of Cu-based bimetallic catalysts for its effective production.

Keywords: CO_2 electroreduction; Cu(100); transition metal doping; ethylene; first principles

1. Introduction

Electrochemically converting carbon dioxide (CO_2) into commodity chemicals or fuels is a promising approach to close the carbon neutral energy loop when utilizing the electricity from renewable power sources[1]. During the reduction processes, CO_2 molecule combined with protons and electrons can be converted into high value-added substances such as carbon monoxide (CO)[2-6], formic acid (HCOOH)[7-10], methane (CH_4)[11-13], ethanol (CH_3CH_2OH)[14, 15] and ethylene (C_2H_4)[16-19]. To date, the regulation of simple single-carbon products including CO and HCOOH has achieved excellent results with Faradaic efficiency nearly 100%, whereas the selectivity towards the formation of multi-carbon products involving more electron transfer such as ethylene and ethanol is still limited. It is highly desirable to improve the Faradaic efficiency of multi-carbon products with high energy density[20, 21].

Hori et al. first reported that copper electrodes could convert CO_2 into hydrocarbons, mainly CH_4 and C_2H_4[22]. Since then the research on the formation of multi-carbons have attracted attention[23, 24], such as C_2H_4, an important intermediate for the synthesis of medicines and high-tech materials[25-27]. The surface orientation of Cu catalyst plays a decisive role in the product selectivity[28]. Generally, the open Cu (100) facet favors the formation of C_2H_4 with low overpotentials in neutral and basic solutions[29, 30]; the close-packed Cu(111) facet favors generating CH_4; and the Cu(110) surface favors the formation of CH_3CH_2OH [31-34]. The formation of C_2H_4 on flat Cu(100) undergoes a key pH-independent CO-CO dimerization process[24, 35-37], where no proton is involved [33]. Nevertheless, the dimerization is difficult to occur on either the terrace Cu(111) or stepped Cu(211)[38-40]. On these two surface sites, the CO intermediates are prone to combine with protons forming COH* or CHO* intermediates (*represents the adsorption site), which can be further protonated and dimerized to yield CH_4 and C_{2+} products, respectively[41, 42]. Although the Cu(100) facet is favorable for C_2H_4 formation, there exists a large energy barrier of about 0.7 eV in the C-C dimerization process[31, 43]. Based on these facts, our work is to cut down the energy barrier by regulating the Cu(100) facet in order to deliver high catalytic selectivity for the C_2H_4 formation.

Doping is an effective avenue to tune the surface electronic structure of metal

catalysts and thus improve the catalytic performance. At present, various Cu-based bimetallic catalysts (alloying with Pb, Pd, Pt, Au, Sn, Zn, In and Cd) have been investigated and shown good properties[44-51]. However, the product selectivity of these bimetallic catalysts is often limited to CO or HCOOH and mainly from the experimental trials. Systematically studying the Cu-based bimetallic catalysts for the CO_2-to-C_2H_4 conversion from a theoretical perspective is urgently needed.

In this work, we have chosen eight different kinds of metal atoms (Zn, Sn, Cd, In, Pd, Fe, Ni, Co) to regulate the electronic properties of Cu(100) facet in light of their different affinities for C and O atoms, namely, different intrinsic activities for CO_2 electroreduction. Specifically, Zn metal is easy to produce CO due to its weaker binding ability to CO; Sn, Cd and In metal are all oxophilic metals that are apt to form OCHO* intermediate to produce HCOOH; Ni, Fe and Pd metal are more likely to generate H_2 due to the stronger binding ability for CO[52, 53]. The reaction energies for the formation of different intermediates on heteroatoms-doped Cu(100) surfaces have been calculated using density functional theory (DFT). Among these catalytic surfaces, the Zn doped one, Zn-Cu(100), demonstrates the best catalytic ability for the C_2H_4 formation. This is due to the adsorption properties of neighboring Cu sites are significantly perturbed by the presence of Zn, and the stronger Zn-O bonding is formed on the catalyst surface, which enhances OCCO evolution. This work may not only give a deep insight into the reaction mechanisms towards C_2H_4 formation on Cu(100) facet, but also provide guidelines for designing Cu-based bimetallic catalysts to effectively produce multi-carbons.

2. Computational details

2.1 Calculation methods

The geometric optimizations, electronic structures and reaction energetics calculations were performed through the spin-polarized DFT method by using Vienna Ab-initio Simulation Package (VASP) code on the basis of the plane-wave pseudopotential[54-57]. The Perdew–Burke–Ernzerhof (PBE) exchange-correlation functional for generalized gradient approximation (GGA)[58] and the projector augmented wave (PAW) method explaining the core-valence interactions were employed. The cutoff energy for plane-wave basis was set to 400 eV, Brillouin-zone integration was performed with a 3×3×1

k-mesh according to the Monkhorst–Pack scheme [59]. The electronic relaxation was performed within an energy tolerance of 10^{-5} eV for self-consistency, while ionic optimizations were performed until all the residual forces were smaller than 0.02 eV/Å. The Fermi-surface effects were handled with the smearing technique of Methfessel and Paxton[60], leveraging a smearing value of 0.02 eV, whereas Gaussian smearing was 0. Cu d^{10} p^1, Zn d^{10} p^2, Fe d^7 s^1, Pd s^1 d^9, Sn s^2p^2, Cd s^2 d^{10}, Co d^8 s^1, Ni d^8s^2 and In s^2p^1 electrons were treated as valence electrons. Spin-polarized wave functions were used for all calculations, which is vital to properly represent the electronic structure of various adsorbed reaction intermediates. In addition, we have set a vacuum region of 20 Å between adjacent images, which is used to impede the interaction along the z direction. Model Cu crystal is a face-centered cubic structure and the calculated equilibrium lattice constant is 3.66 Å, which matches well with theoretical and experimental values of 3.66 Å and 3.62 Å, respectively[61, 62]. We employed the computational hydrogen electrode (CHE) model proposed by Nørskov *et al.* to calculate the change in Gibbs free energy (ΔG) for each elementary step[63], which was defined as follows:

$$\Delta G = \Delta E + \Delta E_{ZPE} - T\Delta S + \Delta G_U + \Delta G_{pH}$$

Here, ΔE is the reaction energy, which can be directly acquired by analyzing the DFT total energies. ΔE_{ZPE} and ΔS are the changes in zero-point energies and entropy, respectively, and T is the system temperature (298.15 K). They are calculated by means of the vibrational frequency. ΔG_U is the contribution of the applied electrode potential (U) to ΔG. $\Delta G_{pH} = 2.303 k_B T \mathrm{pH}$ represents the free energy contribution due to the variations in H concentration, and in this work the pH value is set to be zero for acidic medium. The onset potential (U_{onset}) for the whole reaction is determined by the most positive ΔG (ΔG_{max}), which can be calculated as $U_{onset} = -\Delta G_{max}/e$.

2.2 Model

The computational 3×3×1 periodic cell consisted of 90 atoms modeled by five-layer (100) slabs, which matches the size of experimental materials. Intriguingly, the Cu(100) facet is a smooth facet containing a lower surface density of metal atoms and 4-fold binding sites, and the corresponding model is shown in **Figure 1a and 1b**. Thereafter, we constructed the Zn-Cu(100) model by replacing a Cu atom on the intact Cu(100) surface with a Zn atom (**Figure 1c and 1d**). In order to judge the bonding type of the surface atoms after doping and the characteristics of localized distribution of electrons, we plotted the electron localization function (ELF) of Zn-Cu(100). By definition, the value of ELF is between 0 and 1: ELF = 1 indicates perfect localization of electrons; ELF = 0.5 represents that the electrons form electron-gas-like pair probability; and ELF = 0 means the absence of electrons. By analyzing **Figure 1e**, we found that the locality

of electrons was low, near free distribution over the whole metal crystal, the maximum value of ELF was only 0.315. Therefore, the electrons in this section were delocalized that was in line with the metal bond. That is to say, the doped transition metal Zn formed metal bond with the nearest Cu atoms. The same methodology was applied for other heteroatom-doped systems. In fact, the real surface is supposed to be only one face in contact with the vacuum considering the actual model. When adsorption occurs, only the outermost atoms that are in contact with the vacuum layer have changed. The underlying atomic layer should be fixed at the position of the bulk material and only let the upper layers of atoms move when optimizing. Therefore, we fixed the bottom three layers of the structure, and left the top two layers and the adsorbates to relax.

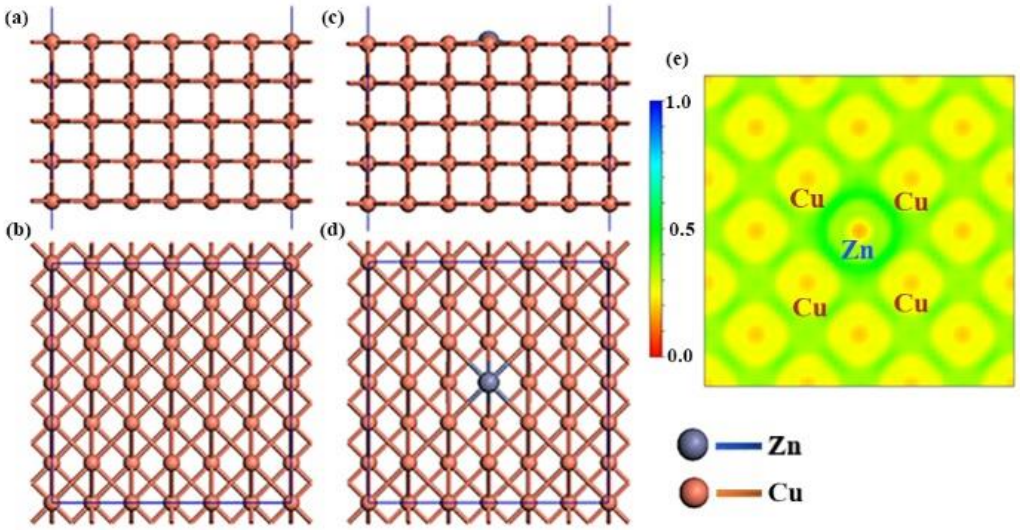

Figure 1 (a) and (b) are the main view and top view of pure-Cu(100), respectively. (c) and (d) are the main view and top view of Zn-Cu(100), respectively. The orange ball represents the Cu atom, and the dark blue ball represents the Zn atom. (e) presents the electron localization function of Zn-Cu(100).

Considering that the Zn-Cu(100) has the best performance in reducing CO_2 to C_2H_4, we calculated the band structure and density of state (DOS) of Cu(100) and Zn-Cu(100) as well as analyzed the electronic properties changes caused by the doping (**Figure 2**). Since the electronic status approaching to Fermi energy has a major influence on the material, the deep-level electronic status is not taken into consideration. The DOS of pure Cu(100) is revealed in **Figure 2b**, which clearly demonstrates that the energy levels were mainly provided by Cu-p orbits. **Figure 2d** shows the DOS of Zn-Cu(100), the peak value of DOS for the d orbits, p orbit and s orbits of Zn atom was extremely low because there was only one Zn atom. However, the DOS of Zn-Cu(100)-Total was the total contribution from all energy bands containing 90 atoms. In order to clearly

analyze the DOS of Zn atom in this energy range, we presented the expanded view(inset of **Figure d**). Clearly, the p orbit and s orbit of Zn atom approaching to Fermi level played a major role, especially the p orbit of Zn, while the d orbit of Zn had no contribution. Despite that there is no band gap in either Cu(100) or Zn-Cu(100) (**Figure 2a and 2c**), the introduction of Zn metal made new orbits appearing at the Fermi level, and it would hybridize with the orbit of Cu to form a new electronic state, which is beneficial for electronic transitions. **Figure 2b** and **2d** reveal that the distribution of DOS peaks was uneven and localized in the selected energy range, which is consistent with the strong electronic locality of d-orbit.

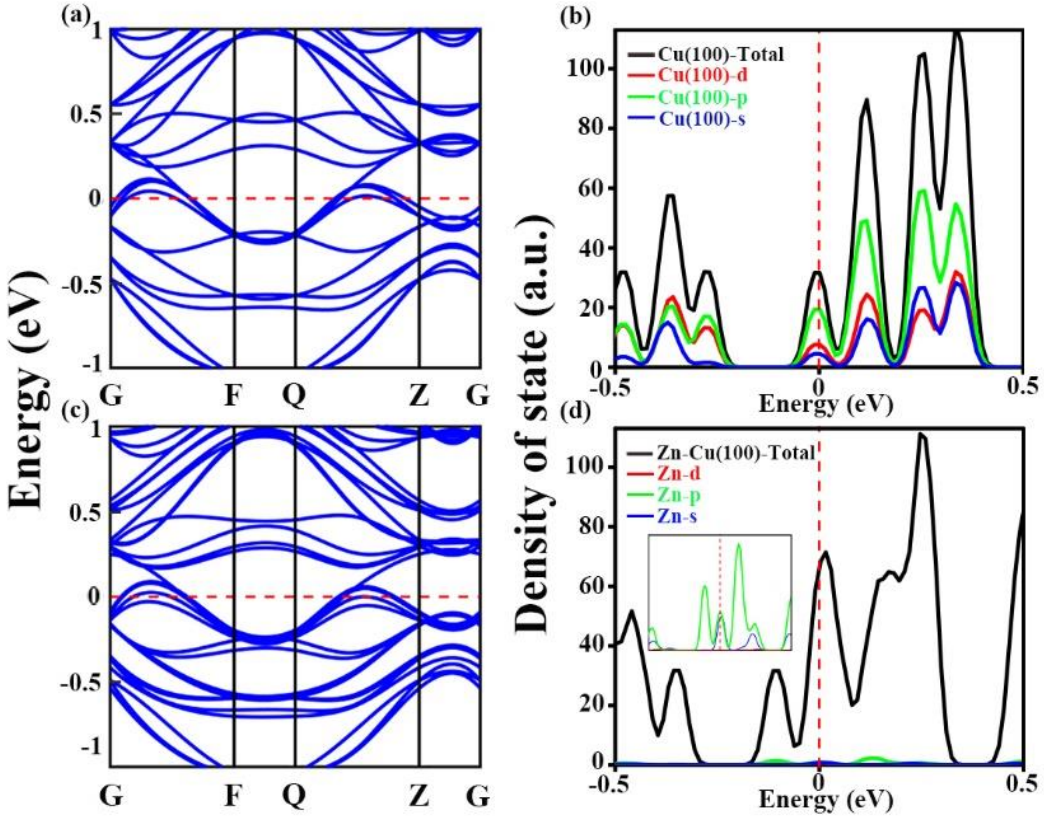

Figure 2. (a, b), band structure and density of state for pure Cu(100); (c, d), band structure and density of state for Zn-Cu(100). The small image in **Figure d** is an enlargement of Zn orbits within the energy range. Dotted lines match along with the Fermi level.

2.3 Path

Electrocatalytic reduction of CO_2 to C_2H_4 consume 12 electrons. **Figure 3** shows the path map of the reaction, which has been widely recognized [43, 64-69]. In this chart, there are three waters (H_2O) and one C_2H_4 produced throughout the reaction. Interestingly, only 10 protons and electrons were shown in the path diagram, while the other two

protons and electrons were consumed in CO*CO*, involving two CO*. Here the C-C dimerization was considered as a coupling process between CO* and CO* rather than a coupling process between CO gas and CO*. COOH* is a crucial intermediate of producing CO. It cannot be substituted by OCHO*, which produce HCOOH and cannot be further reduced. When all the occupied positions were reacted, a bare adsorption site was left. Then a new cycle of CO_2 coupled with protons and electrons began. Theoretically, the free energy for an ideal hydrogen evolution catalyst is close to 0[63, 70], which is beneficial for the H* adsorption and desorption thus promoting the proton-electron-transfer process.

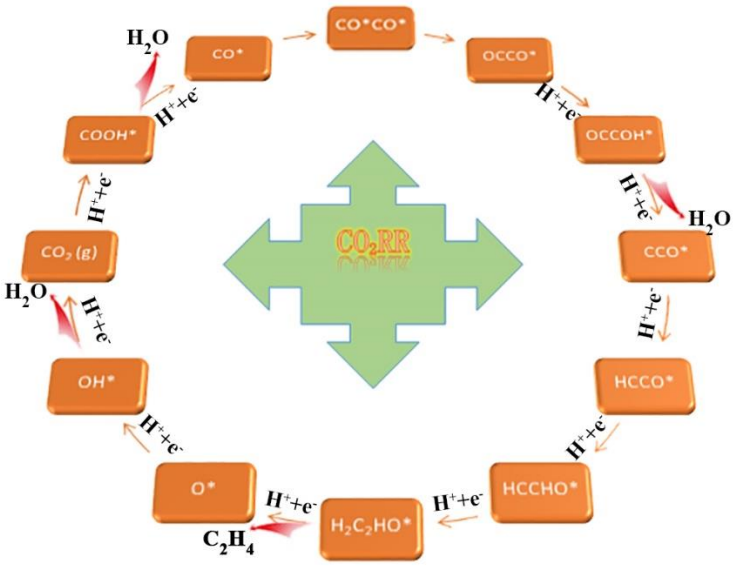

Figure 3. Path diagram of electrocatalytic reduction of CO_2 to C_2H_4 based on Cu(100). Materials in orange model represent the pure Cu(100) or the doped Cu(100).

3. Result and discussion

Although the energy barrier for CO-CO dimerization on Cu (100) has been reported, there exists a big difference in the reported data. Here, in order to provide reliable comparison regardless of the calculation methods or reaction paths, we calculated the energy barrier of each step in the reaction process. **Figure 4a** reveals the energy changes from CO_2 adsorption to C_2H_4 production. Apparently, the non-electrochemical surface reaction of CO*CO* coupling to OCCO* was the rate-limiting step with an energy barrier of 0.71 eV, which is consistent with Calle-Vallejo's report[43]. This energy may be used to overcome the large barriers for the C-C dimerization and

O rotation. In addition, the further hydrogenation of CCO* to HCCO* is also an endothermic process (0.11 eV). It should be pointed out the electron-proton transfer is kinetically favored for other intermediates.

To reduce this energy barrier and promote the reaction kinetics, we doped various metal atoms on Cu(100) surface. It was found that Zn-doped Cu(100) was conducive to the formation of C_2H_4, and the pertinent reaction processes and energy changes are shown in **Figure 4b**. Strikingly, the coupling of CO_2 with proton and electron generated COOH*, where C bound to Zn and O bound to Cu. This process was uphill and the energy barrier of 0.22 eV was the largest in the whole reaction, Clearly, it was a rate-limiting step, therefore a negative electrode potential(-0.22 V) is applied for eliminating the energy barriers of the rate-limiting step. It is worth noting that the protonation of COOH changed from the original exothermic process to an endothermic process due to the doping with Zn atom. It can be inferred that the binding ability of Zn with C was not that strong as with Cu. This can be further confirmed by an energy barrier of 0.16 eV for the formation of CO* indicating a weak CO binding strength on Zn metal, which is consistent with Kuhl's report[71]. The C-C dimerization process for Zn-Cu(100) was still an uphill process. However, its energy barrier was 0.54 eV lower than that of pure Cu(100). The adsorption mode of OCCO was O-bridge adsorption on Zn and C-bridge on Cu, i.e., two atoms in OCCO combined with four atoms on the Zn-Cu(100) surface, while CO* and CO* were linear adsorption. The formed OCCO* yielded OCCOH* via proton-coupled electron transfer. A C-C single bond emerged in OCCOH* species with a length of 1.46 Å, following the generation of CCO* and H_2O with a downhill energy of 1.28 eV. The H_2O desorption readily occurred. This is ascribed to the ease of protonation and subsequent dehydration of OH moieties that makes them more reactive rather than the O atoms in carbonyl moieties. At this point, the bond length between C and C was 1.33 Å, a typical C-C double bond belonging to sp^2 hybridization. These C-C double bonds were retained until the formation of C_2H_4. Subsequently, this α-carbon was protonated to yield HCCO* followed by the generation of HCCHO* via the protonation of C atom in the carbonyl group. The following step was an exothermic reaction with negative energy, yielding H_2C_2HO* via protonation on the α-carbon again.

Since that C bound to Zn and O bound to Cu for $H_2C_2HO^*$, the further producing C_2H_4 and releasing H_2O need to cleave the C-O bond and C-Zn bond as well as remove an *O species. *O could easily couple proton and electron to form *OH in terms of the favorable dynamics. Finally, OH* was protonated to generate H_2O, leaving a clean surface for the next cycle. In summary, the energy barrier of pure Cu(100) for the CO* dimerization was too high to be kinetically favored. After the decorating with Zn, the DOS of the orbital near the Fermi level was significantly increased, which altered the binding of intermediates for achieving an enhanced catalytic ability.

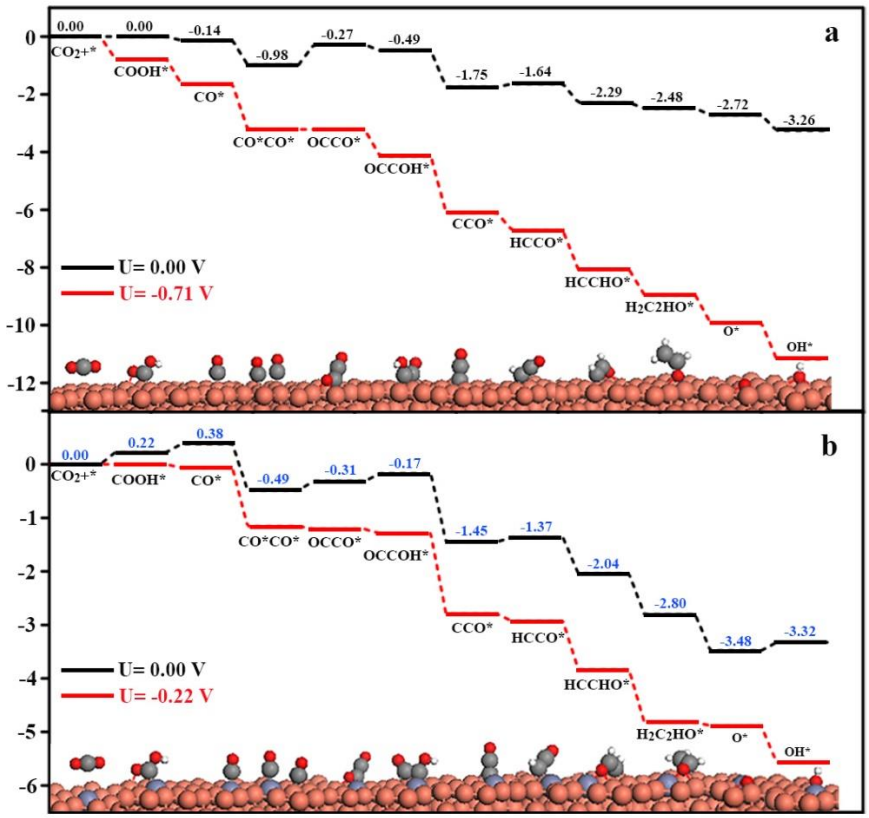

Figure 4. Calculated free energy diagram without (black lines) and with applied potential (red lines) for CO_2 electroreduction on Cu(100): a) pure Cu(100) and b) Zn-Cu(100). Large purple and orange spheres represent Zn and Cu atom, respectively. Small spheres represent O (red), C (gray) and H (white) atoms.

In principle, the incorporation of transition metals into Cu(100) facet can regulate its electronic structure and lower the reaction activation barrier for the C-C dimerization. However, we found only the modification with Zn showed superior catalytic ability to convert CO_2 into C_2H_4 due to its smallest overpotential for the CO_2RR. Generally

speaking, the C-C dimerization was the rate-limiting step of each reaction, but for Sn-Cu(100) the energy barrier was the $H_2C_2HO^*$ protonation to O* and H_2O with a positive energy (1.33 eV), as shown in **Figure 5**. This adsorption occurred via the combination of O and C on the catalyst surface, and the formation of OCCOH* was dynamically favorable. Conversely, the adsorption mode was that when two carbons were combined on the catalyst surface, the coupling of OC-CO* with protons and electron transfer became difficult. Although we commonly believe that the C-C dimerization is the rate-limiting step of the whole reaction, there may be some exceptions. Therefore, we calculated the energy changes of the whole reaction process. Special attention should be paid to the doping with In atom, which was also beneficial to the production of C_2H_4 compared to pure Cu(100). The catalytic activity from easy to difficult was in the order of Zn＞In＞Cd＞Ni＞Sn＞Fe＞Pd＞Co. The generation of COOH* on Cd-Cu(100), In-Cu(100) and Sn-Cu(100) was with higher energy barrier due to their higher oxygen affinity. Those Pd, Fe, Ni, Co doped Cu(100) were facile to form CO* and bound tightly to these catalysts, which is consistent with their strong adsorption capacity for CO on the catalyst surface as poison effect. To sum up, only Zn atom considerably regulated the catalytic performance, as the synergistic effect between Zn and Cu made OCCO tightly bonded to the catalyst surface and effectively lowered the reaction barrier for C-C dimerization. In addition, Figure 5 shows only some key intermediates for seven atoms doped Cu(100). Therefore, in order to understand the reaction process in more detail, we also gave the stable adsorption configurations of each species (Figure S1-S7).

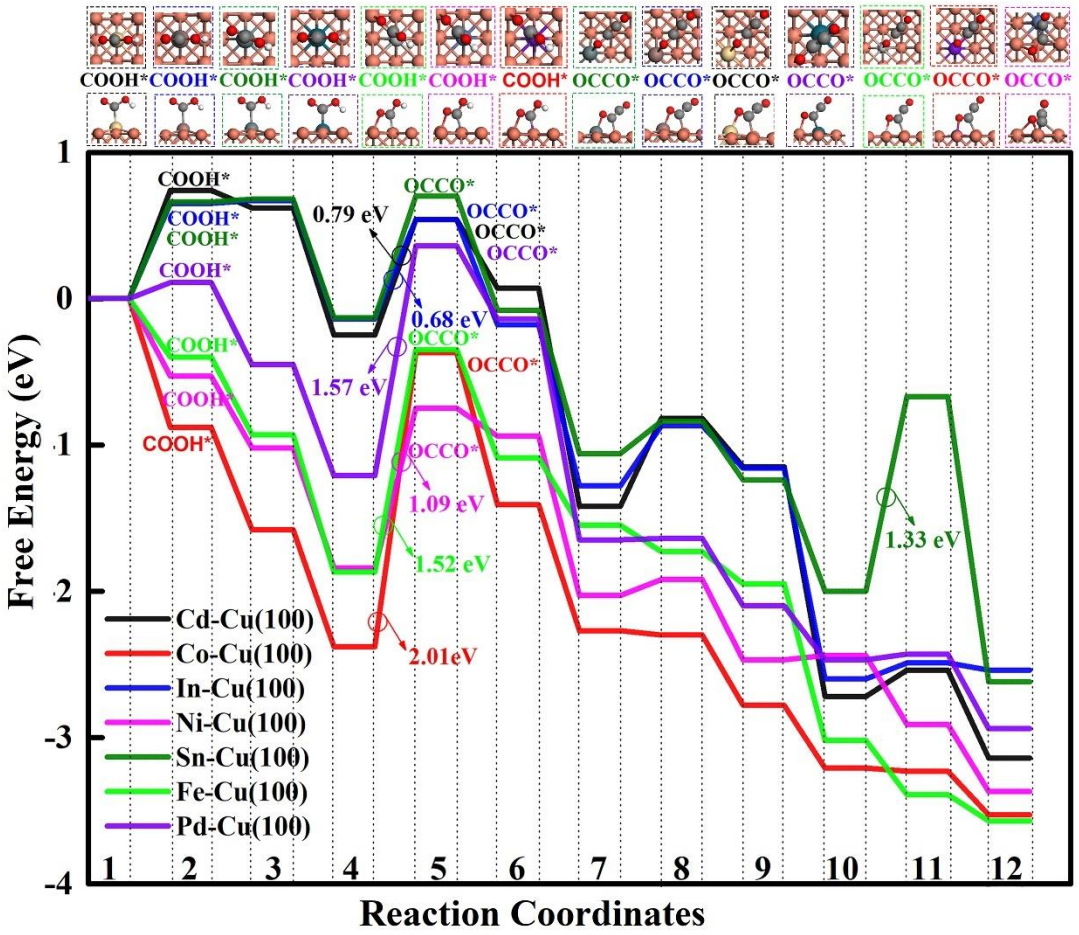

Figure 5. Energy profile of CO_2 reduction reactions for seven atoms doped Cu(100): Cd (black line), Co (red line), In (blue line), Ni (pink line), Sn (dark line), Fe (bright line) and Pd (purple line). The first row and the third row are the top view and main view of COOH* and OCCO* on different metal doped Cu(100) faces, respectively. The color of each font (the second line) corresponds to the doped metal color.

From the energy values above, we can draw a conclusion that there is an interaction between the adsorbates and catalyst, which means there is a charge transfer between them. In order to have a clearer understanding of the mechanism, we plotted the corresponding three-dimensional charge density difference (**Figure 6**). It should be noted that we only calculated the charge density difference of the intermediates with core effect including COOH*, COCO* and OCCO*. Analyzing the pure Cu(100) (picture on the left, **Figure 6**), we found that a large electron cloud existed between COCO and catalyst, indicative of a strong interaction. In contrast, the transfer of charge between OCCO and catalyst was rare, which is in accordance with its higher energy barrier (**Figure 4a**). **Figure 6b, 6e and 6f** display the charge density difference of Zn-Cu(100). Differently, the charge on the surface of the catalyst was redistributed owning

to the doping of Zn atom. The electronic cloud between COOH and the catalyst was relatively small, namely, the transfer of charge was not obvious. It requires to adsorb extra energy to be bound on the catalyst surface. The interaction between OCCO and catalyst became stronger after the doping of Zn metal, making the C-C dimerization more prone to take place.

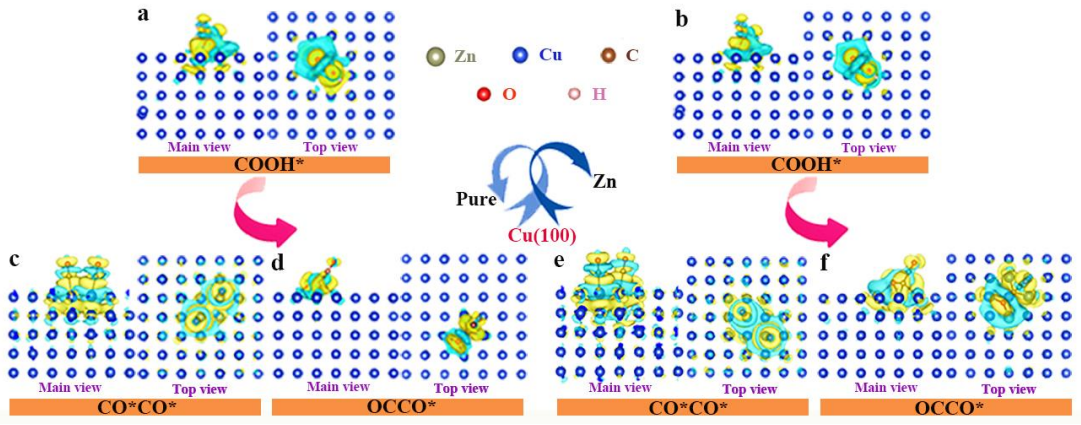

Figure 6. Three-dimensional charge density difference with an isovalue of 0.001 $Å^{-3}$. The charge density difference of COOH*, COCO* and OCCO* species on pure Cu(100) (a, c and d; left side), and Zn-Cu(100) (b, e and f; right side). The yellow electronic cloud indicates charge accumulation and the blue electronic cloud indicates charge depletion. For each intermediate image, its left side is the main view, and the right side is the top view.

Such interaction was further verified by the charge analysis based on the Bader method supplying the quantitative results of charge change of each atom **(Figure 7)**. The O atoms that were bound to the catalyst surface gained electrons, in contrast to the electron loss from the bound Cu atoms or Zn atoms. Obviously this complies with the characteristics of atoms gaining and losing electrons in the periodic table. Furthermore, Cu or Zn when bound to O displayed the strongest ability to loose electrons, especially for the hole-rich Zn species. The introducing of Zn atoms induced the redistribution of the gain and loss of charge for OCCO* **(Figure 7c, 7f)**. Zn atoms lose more electron (0.49 e), which may lead to the improved interaction between Zn and OCCO*. In addition, the C-C bond length of OCCO was 1.34 Å implying the formation of the first C-C double bond.

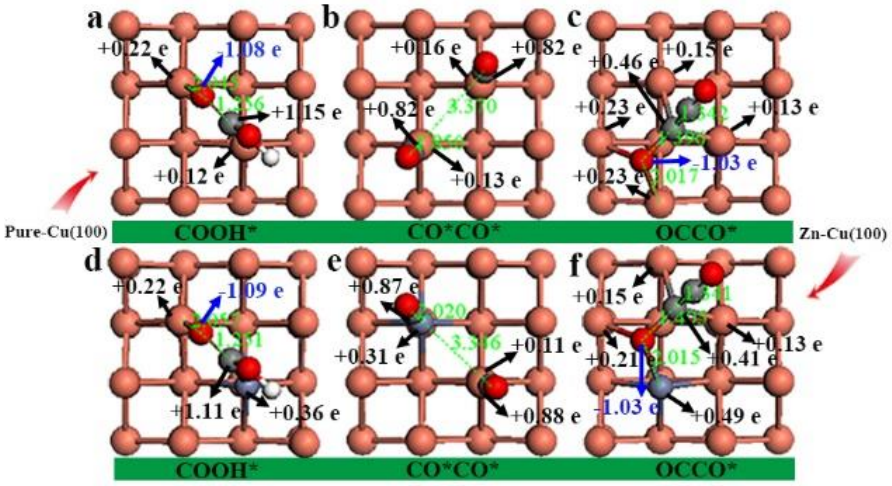

Figure 7. The upper part of the figure is the distance and charge change for COOH*, COCO* and OCCO* on the pure Cu (100), while the lower part is the distance and charge change for COOH*, COCO* and OCCO* on the Zn-Cu(100). The bright green dashed lines and numbers correspond to atoms and distances, separately. The unit of distance is Å. Positive value is electronic loss(black font), negative value is electronic gains(blue font).

To deeply understand the high catalytic activity of Zn-doped Cu(100), we analyzed the projected density of state (PDOS) of various absorbed species on Cu(100) and Zn-Cu(100). Since all the COOH*, CO*CO* and OCCO* bound to the surface of Cu and Zn at the same time, we analyzed the d orbitals of these two atoms Cu and Zn. As shown in **Figure 8**, the energy level in conduction band mainly consisted of the 2p orbits of adsorbed species, while the valence band mainly originated from the 3d orbits of the base atoms. It clearly demonstrates that the hybridization between COOH* and Cu-Cu atoms was stronger than that between COOH* and Zn-Cu atoms. It also implies that the interaction for the former was stronger, which agrees with the reaction energy value (**Figure 4**). Interestingly, the span of state density peak was quite large whether it was in the conduction band or value band **(Figure 8b, 8e).** It indicates that the intermediate CO*CO* had stronger delocalization and stronger bonds with Cu-Cu and Zn-Cu, and hence it was hard for the C-C dimerization. The peak of Cu-Cu and Zn-Cu in the valence band was much higher than the previous peak **(Figure 8c, 8f)**, which is attributed to the combination of OCCO and four atoms of the catalyst surface.

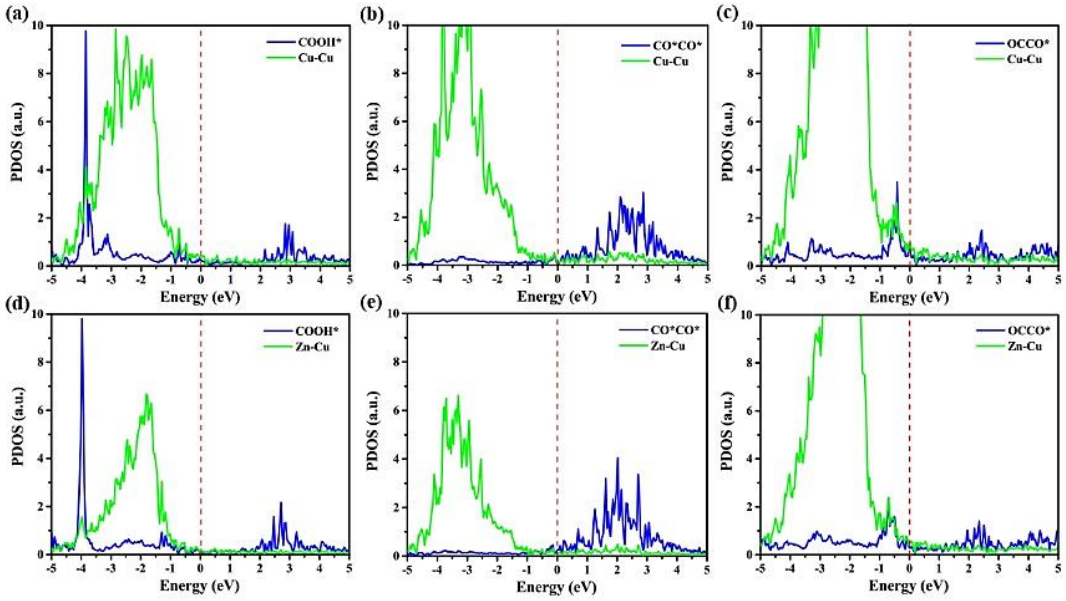

Figure 8. Projected density of state between the intermediates and catalysts. (a-c) and (d-f) are the projected density of state of COOH*, CO*CO* and OCCO* on Cu(100) and Zn-Cu(100), respectively. These projected density of state maps are all spin-up states. The red dashed line corresponds to the Fermi level. Cu-Cu and Zn-Cu represent the atoms that bond with the intermediate.

4. Conclusion

In summary, we ameliorate the performance of the Cu(100) catalysts for the CO_2-to-C_2H_4 conversion by introducing heteroatoms with different intrinsic activities for CO_2 electroreduction (i.e., Zn, Sn, Cd, In, Pd, Fe, Ni and Co). We have calculated the reaction energy of the elementary steps of pure Cu(100) and heteroatoms doped Cu(100) by using DFT method. The results show that the doping of Zn atom significantly lowers the energy barrier for CO dimerization that is considered as the key selectivity-determining step for the CO_2-to-C_2H_4 conversion, and hence improves the electrocatalytic performance. This work provides theoretical insights into the formation processes of C_2H_4 and open an attractive avenue to design highly efficient Cu(100)-based electrocatalysts for producing C_2H_4.

Acknowledgement

This work was supported by the National Natural Science Foundation of China (grant no. 51302079, 51702138), the Natural Science Foundation of Hunan Province (grant no. 2017JJ1008), and the Key Research and Development Program of Hunan Province

of China (No. 2018GK2031). C. Wang thanks the AIIM For Gold Grant (UOW).

Reference

1 N. S. Lewis and D. G. Nocera, *P. Natl. Acad. Sci. USA.,* 2006, **103**, 15729-15735.

2 Y. Mun, S. Lee, A. Cho, S. Kim, J. W. Han and J. Lee, *Appl. Catal. B:Environ.,* 2019, **246**, 82-88.

3 J. L. DiMeglio and J. Rosenthal, *J. Am. Chem. Soc.,* 2013, **135**, 8798-8801.

4 J. Medina-Ramos, R. C. Pupillo, T. P. Keane, J. L. DiMeglio and J. Rosenthal, *J. Am. Chem. Soc.*, 2015, **137**, 5021-5027.

5 S. Rasul, D. H. Anjum, A. Jedidi, Y. Minenkov, L. Cavallo and K. Takanabe, *Angew. Chem. Int. Ed.*, 2015, **54**, 2146-2150.

6 S. Sarfraz, A. T. Garcia-Esparza, A. Jedidi, L. Cavallo and K. Takanabe, *ACS Catal.*, 2016, **6**, 2842-2851.

7 H. Zhong, Y. Qiu, T. Zhang, X. Li, H. Zhang and X. Chen, *J. Mater. Chem.* A, 2016, **4**, 13746-13753.

8 S. Y. Choi, S. K. Jeong, H. J. Kim, I.-H. Baek and K. T. Park, *ACS Sustain. Chem. Eng.,* 2016, **4**, 1311-1318.

9 D. Kopljar, A. Inan, P. Vindayer, N. Wagner and E. Klemm, *J. Appl Electrochem.,* 2014, **44**, 1107-1116.

10 F. Li, L. Chen, G. P. Knowles, D. R. MacFarlane and J. Zhang, *Angew. Chem. Int. Ed.*, 2017, **56**, 505-509.

11 A. A. Peterson and J. K. Nørskov, *J. Phys. Chem. Lett.,* 2012, **3**, 251-258.

12 M. K. Kim, H. J. Kim, H. Lim, Y. Kwon and H. M. Jeong, *Electrochim. Acta*, 2019, **306**, 28-34.

13 Y. Wang, Z. Chen, P. Han, Y. Du, Z. Gu, X. Xu and G. Zheng, *ACS Catal*, 2018, **8**, 7113-7119.

14 J. Yuan, L. Liu, R.-R. Guo, S. Zeng, H. Wang and J.-X. Lu, *Catalysts*, 2017, **7**.

15 S. Lee, G. Park and J. Lee, *ACS Catal*, 2017, **7**, 8594-8604.

16 C.-T. Dinh, T. Burdyny, M. G. Kibria, A. Seifitokaldani, C. M. Gabardo, F. P. G. de Arquer, A. Kiani, J. P. Edwards, P. De Luna, O. S. Bushuyev, C. Zou, R. Quintero-Bermudez, Y. Pang, D. Sinton and E. H. Sargent, *Science*, 2018, **360**, 783-787.

17 D. Wu, C. Dong, D. Wu, J. Fu, H. Liu, S. Hu, Z. Jiang, S. Z. Qiao and X.-W. Du, *J. Mater. Chem.* A, 2018, **6**, 9373-9377.

18 S. Ma, M. Sadakiyo, R. Luo, M. Heima, M. Yamauchi and P. J. A. Kenis, *J. Power Sources,* 2016, **301**, 219-228.

19 C. Reller, R. Krause, E. Volkova, B. Schmid, S. Neubauer, A. Rucki, M. Schuster and G. Schmid, *Adv. Energy. Mater.*, 2017, **7,** 1602114.

20 A. Keskin and M. Gürü, *Energy Sources*, 2011, **33**, 2194-2205.

21 A. Shota, H. Taizo and J. C. Liao, *Nature*, 2008, **451**, 86-89.

22 Y. Hori, K. Kikuchi, A. Murata and S. Suzuki, *Cheminform*, 1986, **17**, 897-898.

23 L. Ronald, *J. Electrochem. Soc.*, *1987,* **134**, 1873-1874.

24 K. J. P. Schouten, Y. Kwon, C. J. M. van der Ham, Z. Qin and M. T. M. Koper,

Chem. Sci., 2011, **2**, 1902.
25 Y. Yao, D. J. Graziano, M. Riddle, J. Cresko and E. Masanet, *Environ. Sci. Technol.,* 2015, **49**, 14704-14716.
26 J. Hong, Y. Zhang, X. Xu and X. Li, *Biomass & Bioenergy*, 2014, **67**, 304-311.
27 J.-Y. Park, Y.-J. Lee, K.-W. Jun, J. W. Bae, N. Viswanadham and Y. H. Kim, *J. Ind. Eng. Chem.*, 2009, **15**, 847-853.
28 Y. Hori, I. Takahashi, O. Koga and N. Hoshi, *J. Phys. Chem. B*, 2002, **106**, 15-17.
29 Y. Hori, I. Takahashi, O. Koga and N. Hoshi, *J. Mol. Catal. A:Chem.*, 2003, **199**, 39-47.
30 K. J. P. Schouten, Z. Qin, E. P. Gallent and M. T. M. Koper, *J. Am. Chem. Soc.*, 2012, **134**, 9864-9867.
31 Y. Huang, A. D. Handoko, P. Hirunsit and B. S. Yeo, *ACS Catal.*, 2017, **7**, 1749-1756.
32 F. S. Roberts, K. P. Kuhl and A. Nilsson, *Angew. Chem. Int. Ed.*, 2015, **54**, 5179-5182.
33 F. S. Roberts, K. P. Kuhl and A. Nilsson, *ChemCatChem*, 2016, **8**, 1119-1124.
34 K. J. Schouten, Z. Qin, E. Perez Gallent and M. T. Koper, *J. Am. Chem. Soc.*, 2012, **134**, 9864-9867.
35 A. D. Handoko, F. Wei, Jenndy, B. S. Yeo and Z. W. Seh, *Nat. Catal.*, 2018, **1**, 922-934.
36 L. Ou, W. Long, Y. Chen and J. Jin, *RSC Adv.*, 2015, **5**, 96281-96289.
37 Z.-Y. Chang, S.-J. Huo, J.-M. He and J.-H. Fang, *Surf. and Interfaces*, 2017, **6**, 116-121.
38 K. Jiang, R. B. Sandberg, A. J. Akey, X. Liu, D. C. Bell, J. K. Nørskov, K. Chan and H. Wang, *Nat. Catal.*, 2018, **1**, 111-119.
39 J. H. Montoya, C. Shi, K. Chan and J. K. Nørskov, *J. Phys. Chem. Lett.,* 2015, **6**, 2032-2037.
40 H. Li, Y. Li, M. T. M. Koper and F. Calle-Vallejo, *J. Am. Chem. Soc.*, 2014, **136**, 15694-15701.
41 J. H. Montoya, A. A. Peterson and J. K. Nørskov, *ChemCatChem*, 2013, **5**, 737-742.
42 A. A. Peterson and J. K. Nørskov, *J. Phys. Chem. Lett.*, 2012, **3**, 251-258.
43 F. Calle-Vallejo and M. T. Koper, *Angew. Chem. Int. Ed.*, 2013, **52**, 7282-7285.
44 J. He, N. J. J. Johnson, A. Huang and C. P. Berlinguette, *ChemSusChem*, 2018, **11**, 48-57.
45 E. Andrews, Y. Fang and J. Flake, *J. Appl. Electrochem.*, 2018, **48**, 435-441.
46 H. Hu, Y. Tang, Q. Hu, P. Wan, L. Dai and X. J. Yang, *Appl. Surf. Sci.*, 2018, **445**, 281-286.
47 X. Zhao, B. Luo, R. Long, C. Wang and Y. Xiong, *J. Mater. Chem. A*, 2015, **3**, 4134-4138.
48 C. Wang, M. Cao, X. Jiang, M. Wang and Y. Shen, *Electrochim. Acta*, 2018, **271**, 544-550.

49 Y. J. Jang, J. Lee, J. H. Kim, B. J. Lee and J. S. Lee, *J. Power Sources*, 2018, **378**, 412-417.

50 W. Zhu, L. Zhang, P. Yang, X. Chang, H. Dong, A. Li, C. Hu, Z. Huang, Z.-J. Zhao and J. Gong, *Small*, 2018, **14**, 1703314.

51 Y. Ge, H. Abe, R. Kodiyath, S. Ueda and M. Miyauchi, *J. Mater. Chem. A*, 2017, **5**, 12113.

52 K. P. Kuhl, H. Toru, E. R. Cave, D. N. Abram, K. Jakob and T. F. Jaramillo, *J. Am. Chem. Soc.*, 2014, **136**, 14107-14113.

53 Y. Hori, *Modern Aspects of Electrochemistry*, 2008, **42**, 89-189.

54 G. Kresse, *Phys. Rev. B: Condens. Matter.*, 1993, **48**, 13115-13118.

55 G. Kresse and J. Furthmüller, *Comp. Mater. Sci.*, 1996, **6**, 15-50.

56 G. Kresse and J. Furthmuller, *Phys. Rev. B: Condens. Matter.*, 1996, **54**, 11169-11186.

57 G. Kresse and J. Hafner, *Phys. Rev. B: Condens. Matter.*, 1994, **49**, 14251-14269.

58 J. P. Perdew, J. A. Chevary, S. H. Vosko, K. A. Jackson, M. R. Pederson, D. J. Singh and C. Fiolhais, *Phys. Rev. B: Condens. Matter.*, 1992, **46**, 6671-6687.

59 H. J. Monkhorst and J. D. Pack, *Phys. Rev. B*, 1976, **13**, 5188-5192.

60 M. Methfessel and A. T. Paxton, *Phys. Rev. B*, 1989, **40**, 3616-3621.

61 J. Greeley, A. A. Gokhale, J. Kreuser, J. A. Dumesic, H. Topsoe, N. Y. Topsoe and M. Mavrikakis, *J. Catal*, 2003, **213**, 63-72.

62 CRC Handbook of Chemistry and Physics, 76th ed., *CRC Press*, New York, 1996.

63 A. A. Peterson, F. Abild-Pedersen, F. Studt, J. Rossmeisl and J. K. Nørskov, *Energ. Environ. Sci.*, 2010, **3**, 1311-1315.

64 J. Wang, Z. Li, C. Dong, Y. Feng, J. Yang, H. Liu and X. Du, *ACS Appl. Mater. Interfaces*, 2019, **11**, 2763-2767.

65 D. Gao, I. T. McCrum, S. Deo, Y.-W. Choi, F. Scholten, W. Wan, J. G. Chen, M. J. Janik and B. Roldan Cuenya, *ACS Catal.*, 2018, **8**, 10012-10020.

66 J. Zhao, Z. Chen and J. Zhao, *J. Mater. Chem. A*, 2019, **7**, 4026-4035.

67 J. H. Montoya, C. Shi, K. Chan and J. K. Nørskov, *J. Phys. Chem. Lett.*, 2015, **6**, 2032-2037.

68 K. J. P. Schouten, E. Pérez Gallent and M. T. M. Koper, *J. Electroanal. Chem.*, 2014, **716**, 53-57.

69 S. Hanselman, M. T. M. Koper and F. Calle-Vallejo, *ACS Energy Lett.*, 2018, **3**, 1062-1067.

70 A. A. Peterson and J. K. Nørskov, *J. Phys. Chem. Lett.*, 2012, **3**, 251-258.

71 K. P. Kuhl, T. Hatsukade, E. R. Cave, D. N. Abram, J. Kibsgaard and T. F. Jaramillo, *J. Am. Chem. Soc.*, 2014, **136**, 14107-14113.

Zn-Doped Cu(100) Facet with Efficient Catalytic Ability for CO_2 Electroreduction to Ethylene

Yuefeng Zhang, [†a] Yong Zhao, [†b] Caiyun Wang, [b,*] Zengxi Wei, [a] Jianjun Liu, [a] Quanhui Liu, [a] Pengbin He, [a] Jianmin Ma [a,c,*]

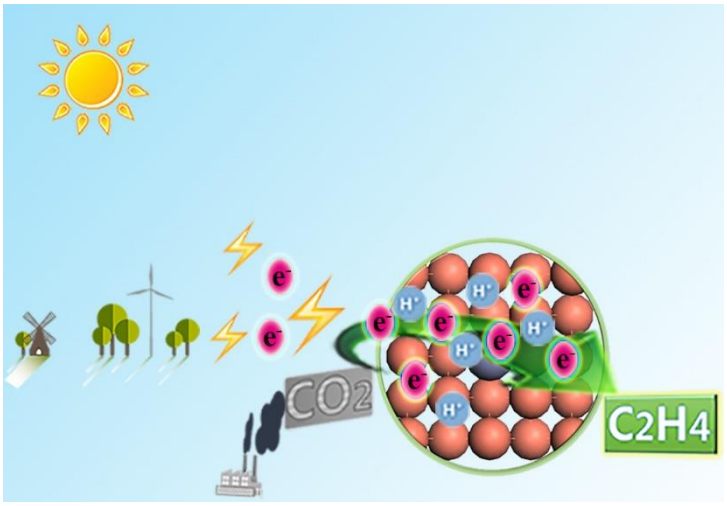

Theoretical calculations demonstrate that Zn-doped Cu(100) facet possesses efficient catalytic ability for the CO_2-to-C_2H_4 conversion. This work provides deep insights into the formation mechanism of C_2H_4 on transition metal doped Cu surface.